THERMAL-MECHANICAL MODELING OF STAINLESS STEEL FORGINGS[*]

ARTHUR A. BROWN, TIMOTHY D. KOSTKA, BONNIE R. ANTOUN, MICHAEL L. CHIESA, DOUG J. BAMMANN[+], STEPHANIE A. PITTS[++], STEPHEN B. MARGOLIS, DEVIN O'CONNOR, NANCY Y.C. YANG

SANDIA NATIONAL LABORATORIES, LIVERMORE, CA 94551
aabrown@sandia.gov

[+]MISSISSIPPI STATE UNIVERSITY, MS 39762

[++]WASHINGTON STATE UNIVERSITY, PULLMAN, WA 99164

ABSTRACT

A constitutive model for recrystallization has been developed within the framework of an existing dislocation-based rate and temperature-dependent plasticity model. The theory has been implemented and tested in a finite element code. Material parameters were fit to data from monotonic compression tests on 304L steel for a wide range of temperatures and strain rates. The model is then validated by using the same parameter set in predictive thermal-mechanical simulations of experiments in which wedge forgings were produced at elevated temperatures. Model predictions of the final yield strengths compare well to the experimental results.

1. Introduction

During high temperature manufacturing processes, metals undergo microstructural changes that can greatly affect material properties and residual stresses. Some of the physical mechanisms that influence the strength of a material are strain hardening, recovery, recrystallization, and grain growth (1,2). If the deformation conditions such as temperature and strain rate are not controlled properly during forging, welding, rolling, or other processes, the final part may have inadequate strength or residual stresses that could be detrimental to the life of the part (3). In order to be able to optimize manufacturing processes using computational capabilities, it is necessary to have a physically-based constitutive model that captures the dominant strengthening and softening mechanisms. Such a model with predictive capabilities can be used in an optimization scheme to reduce the number of design iterations required to produce a part that meets all strength and microstructural requirements.

Recrystallization is a complex, inhomogeneous process in which nucleation and growth of new strain-free grains replace the worked microstructure of a strained material (4,5). Recrystallization is due to the motion of grain and subgrain boundaries. As the boundaries move, they sweep away the dislocation structure, leaving a strain-free material with a very low dislocation density. The nucleation of a new recrystallized grain is believed to be due to the growth of an existing deformation-induced subgrain (6). At elevated temperatures, a subgrain with a lower level of stored energy will preferentially expand at the expense of neighboring subgrains. The driving force for recrystallization is the difference in energy between the deformed and recrystallized state (7). If the expanding subgrain reaches a critical size, it becomes a stable recrystallized grain.

In (8), a constitutive model for static and dynamic recrystallization was developed in which no critical criterion was utilized to initiate recrystallization. Rather, the kinetics of recrystallization are modeled based on the mobility of grain and subgrain boundaries under the driving force provided by the stored energy in the dislocation structure.

In this paper, coupled thermal-mechanical simulations are performed, including the effects of die chill, heat generated due to plastic dissipation, and conduction and strength evolution that occurs after compression but before quenching. Uncertainties in processing conditions were considered and propagated through the simulations to determine uncertainties in final predicted strengths.

A simplified version of the model is presented in the next section since we are primarily concerned with static recrystallization for high-rate forgings. Parameter optimization is then discussed. Finally, a comparison between model predictions and experimental results is provided.

2. Constitutive Model

A treatment of the kinematics and thermodynamics of the model is documented in a full-length manuscript under review (9). The constitutive model is explained in detail in (8). Here, for simplicity, a condensed treatment of the constitutive model is given for the simplified case of uniaxial stress.

For uniaxial stress, let σ represent the only non-vanishing component of the Cauchy stress tensor and ε represent the axial component of the Eulerian strain tensor. After making approximations for small elastic strains, it can be shown that the model reduces to the following set of equations, written here in the current configuration:

$$\dot{\sigma} = E\left(\dot{\varepsilon} - \dot{\varepsilon}^{p}\right) \tag{1}$$

$$\dot{\varepsilon}^{p} = c\left(\sinh\left[\left\langle \frac{\sigma}{\kappa + Y(\theta)} - 1 \right\rangle\right]\right)^{n(\theta)} \tag{2}$$

$$\kappa = \kappa_{1-X}\left(1 - X\right) \tag{3}$$

$$\dot{\kappa}_{1-X} = \left[H(\theta)\left(1 + \frac{\overline{\zeta}_{1-X}}{\overline{\kappa}_{1-X}}\right) - R_d(\theta)\kappa_{1-X}\right]\left|\dot{\varepsilon}^p\right| \qquad [4]$$

$$\dot{\zeta}_{1-X} = h_\zeta \zeta_{1-X}^{1-1/r}\left|\dot{\varepsilon}^p\right| \qquad [5]$$

$$\dot{X} = \frac{1}{\mu\theta}e^{-\frac{c_\theta}{\theta}}\left(1 - e^{-B\overline{\zeta}_{1-X}^m}\right)\left[c_{\overline{\kappa}}\overline{\kappa}_{1-X}^2 + c_{\overline{\zeta}}\overline{\zeta}_{1-X}^2\right]X^a\left(1 - X\right)^b \qquad [6]$$

$$\dot{\theta} = \frac{\beta}{\rho c_p}\sigma\dot{\varepsilon}^p \qquad [7]$$

Equations [1] and [2] provide the elasticity relation and the flow rule for the plastic strain rate. Equation [3] averages the isotropic hardening variable, κ, between the unrecrystallized and recrystallized volume fractions, where the isotropic hardening variable in the recrystallized volume fraction is assumed to be zero. Equation [4] is the evolution equation for the isotropic hardening variable in the unrecrystallized volume fraction, which has a hardening minus recovery format based on (10). The hardening rate increases as the subgrain boundary spacing, represented by the misorientation variable ζ, decreases. Equation [5], based on (11), tracks the misorientation variable, ζ_{1-X}, in the unrecrystallized volume fraction. ζ_{1-X} is inversely related to the average spacing between geometrically necessary boundaries. Equation [6] describes the kinetics of recrystallization through a variable representing the volume fraction of recrystallized material, X. The stored energy due to the dislocation structure, represented by κ_{1-X} and ζ_{1-X}, drives the recrystallization kinetics. The mobility of subgrain boundary motion increases with misorientation angle, which increases as the spacing between geometrically necessary boundaries decreases. The last equation tracks the evolution of temperature due to adiabatic heating. Here, it is assumed that $\beta = 0.95$, i.e. 95% of the plastic work is dissipated as heat. In this work, coupled thermal-mechanical simulations are performed in which the constitutive model calculates the heat generated due to plastic work, which is passed to the thermal code for use as a source term in the energy equation. Thus the temperature will also change due to conduction, radiation, and convection.

The model in this form is only valid for static recrystallization, where the isotropic hardening variable in the recrystallized volume fraction is assumed to be zero. For dynamic recrystallization, the recrystallized material will continue to harden with increased strain. For a treatment of the model form capable of both static and dynamic recrystallization, see (8).

3. Model Performance

Material parameters were fit to data from monotonic compression tests on 304L steel for a wide range of temperatures and strain rates. Three types of test data were included in the set used for parameter optimization. Stress-strain data from single-stage compression at constant strain rate is shown in Figure 1. The plot legends show the

initial specimen temperature. During straining at high rates, the temperature increases somewhat due to plastic dissipation. Figure 2 shows stress-strain data from two-stage compression tests. For each specimen, the first stage of compression was performed at elevated temperature, followed by a quench after approximately five seconds. The second compression stage was conducted at room temperature. Figure 3 contains recrystallized volume fraction data from single-stage compressions tests followed by various hold times before quenching. The data was determined from microstructure from etched samples of the compression specimens.

Model parameters were optimized using the three types of data discussed above (see Appendix). The results are shown in Figures 1 through 3. The model captures the material response quite well over the full range of temperatures and strain rates.

4. Validation

The theory has been implemented and tested in Arpeggio, Sandia's code coupling of an implicit quasistatics code, Adagio (12), with a thermal code, Aria (13). The model is then validated by using the same parameter set in predictive simulations of experiments in which 304L stainless steel wedges were forged with a HERF machine at Precision Metal Products, Inc. (PMP). Two wedge geometries, shown in Figure 4, were forged at 1500F and 1600F. For each forging, the wedge heated in a furnace to the nominal temperature, then transferred to a flat die, and compressed to a final height of one inch by a platen traveling at a rate of approximately 20 ft/s. The forging was then transferred to a quench bath. From the flattened forgings, tensile specimens were machined and tested. Figure 5 shows the locations of the tensile specimens. For all wedges, specimen A was taken one inch to the right of the initially-tapered edge. The spacing between each specimen location was 0.52" for the short wedges and 0.64" for the tall wedges.

A set of simulations were performed to account for uncertainties in the input parameters. Due to time constraints, for each nominal case, simulations were done to provide upper and lower bounds on the expected final yield strengths at the six specimen locations. The uncertainties were based on measurements taken at PMP during forgings of different geometries. The ingot temperature when transferred from the furnace is assumed to be within +-20F of nominal. Radiation and convection were modeled for the estimated transfer time of 1.7 to 3.7 seconds. Conduction to the die was also modeled for 2.8 to 4.9 seconds before compression began. After the wedge is flattened at 20 ft/s, conduction occurs for 0.5 to 2 seconds before the wedge is removed for transfer to the quench bath, which takes between 3 to 4.8 seconds. To account for the uncertainty in the coefficient of friction, we ran the full suite of experiments once with a coefficient of friction of 0.1 and once with frictionless contact.

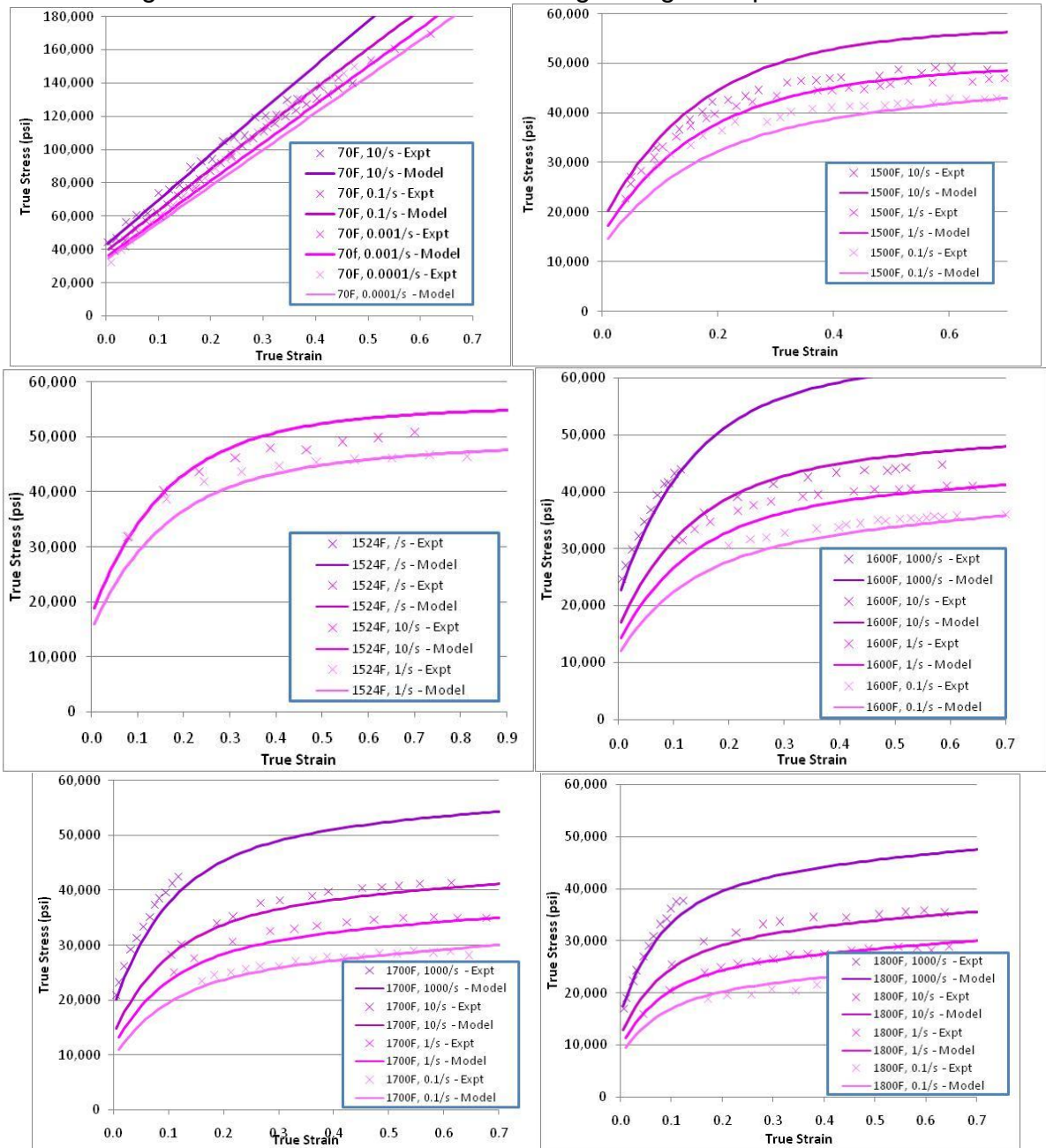Figure 1. Stress-strain data from single-stage compression tests.

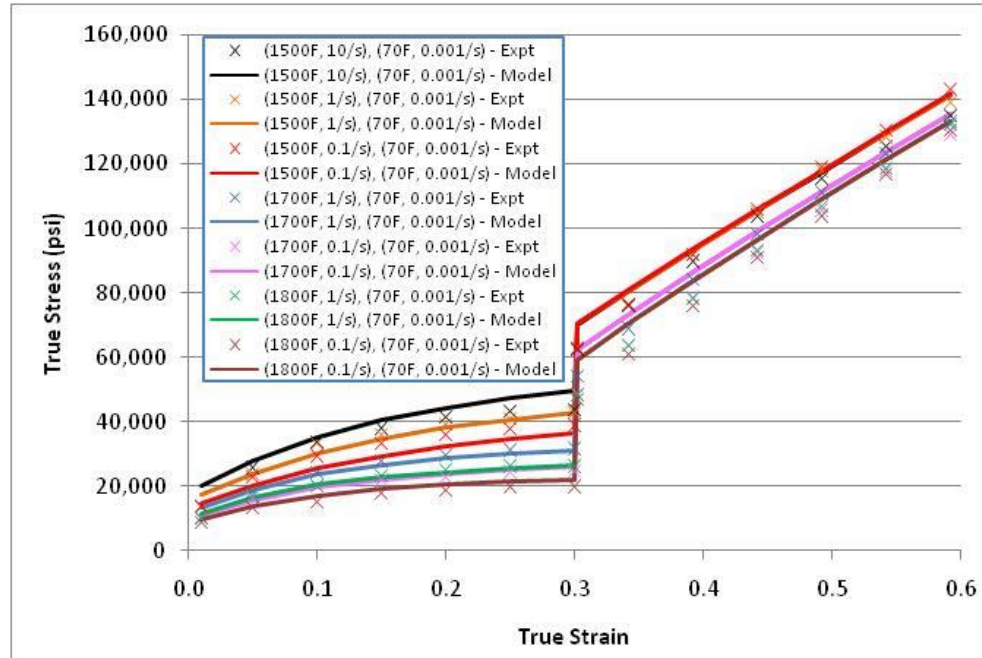Figure 2. Stress-strain data from two-stage compression tests.

Figure 3. Recrystallized volume fraction data from compress-and-hold tests.
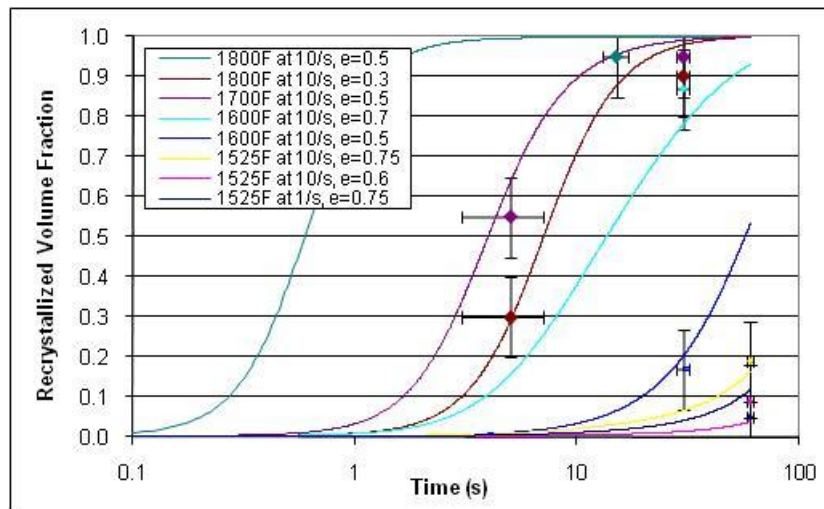
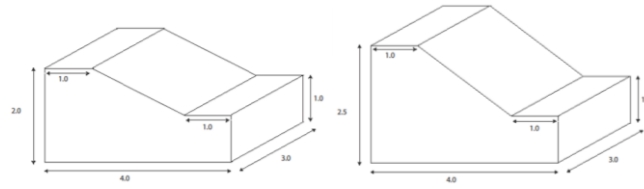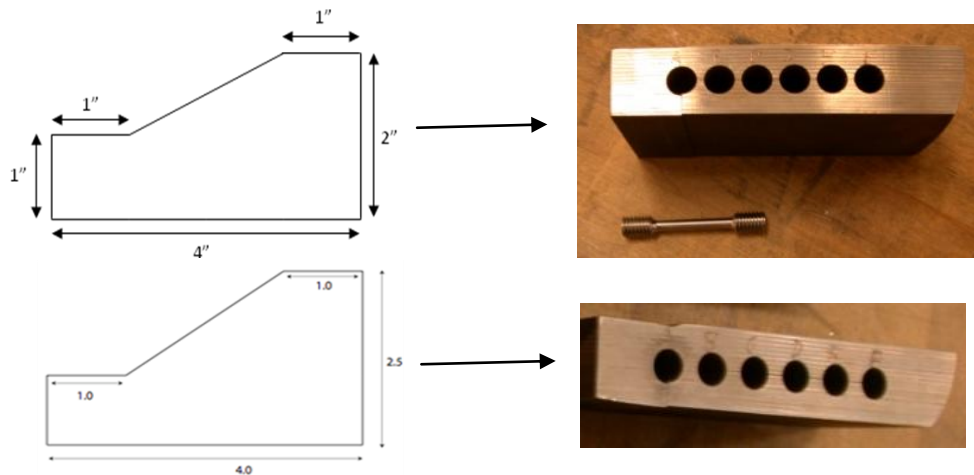Figure 4. Dimensions of the short and tall wedge designs.

Figure 5. Locations of the tensile specimens for the short and tall wedge designs.

The plastic strain contours for a typical run (in this case, 1580F for the tall wedge with a coefficient of friction of 0.1) are plotted in Figure 6. The plastic strain increases as one moves from position "A" to position "F". The dislocation density increases with plastic strain, as does the average misorientation angle across deformation-induced subgrain boundaries. The rate of recrystallization increases with dislocation density and misorientation angle, so the recrystallized volume fraction increases from position "A" to position "F" (see Figure 7).

The final room-temperature, quasistatic yield strength predictions for the short and tall wedges are plotted in Figures 8 and 9, respectively. The range of yield strengths predicted by the simulations based on the uncertainties in the input parameters are depicted by error bars; the experimental measurements are represented by "x" symbols. Since recovery and recrystallization are thermally activated processes, the final strengths of 1500F forgings are higher than the 1600F forgings. As strain increases (e.g. over positions A, B, and C), strength increases due to additional work hardening. However, if the temperature is high enough, the additional work hardening can induce recrystallization, which causes the strength to drop at higher strains (e.g. over positions D, E, and F). The simulations capture the general trends in the data very well. The error in final yield strength predictions is plotted in Figure 10. For cases in which the experimental value lies within the prediction bounds, the error is zero. Otherwise, the

error is calculated as the difference between the closest prediction bound and the experimental value, normalized by the experimental value.

The uncertainties in the yield strength predictions are largest for higher temperature and higher strains because those conditions induce a higher rate of recrystallization. When the rate of recrystallization is high, uncertainty in time before quenching causes uncertainty in the amount of recrystallization that occurs (see Figure 3) and hence in the final strength.

Figure 6. Plastic strain contour plot for the tall wedge at initial temperature of 1580F.
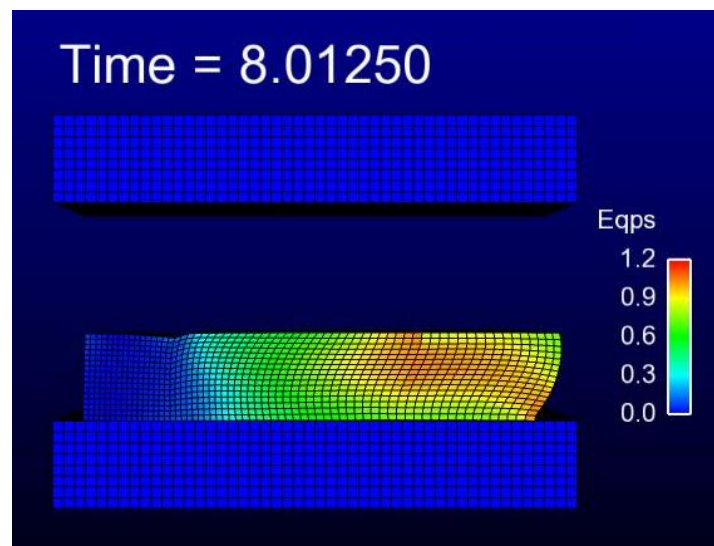

Figure 7. Contour plot of the recrystallized volume fraction for the tall wedge at initial temperature of 1580F.
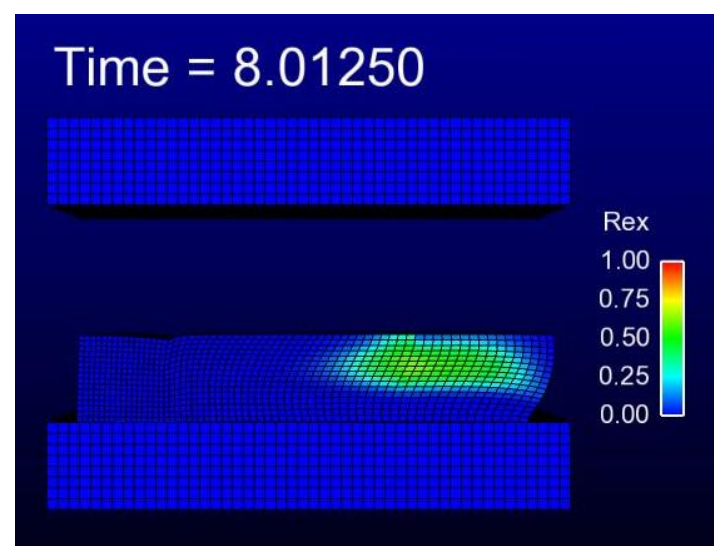
Figure 8. Final yield strengths at locations A through F of the short wedge, based on simulation predictions and experiments.
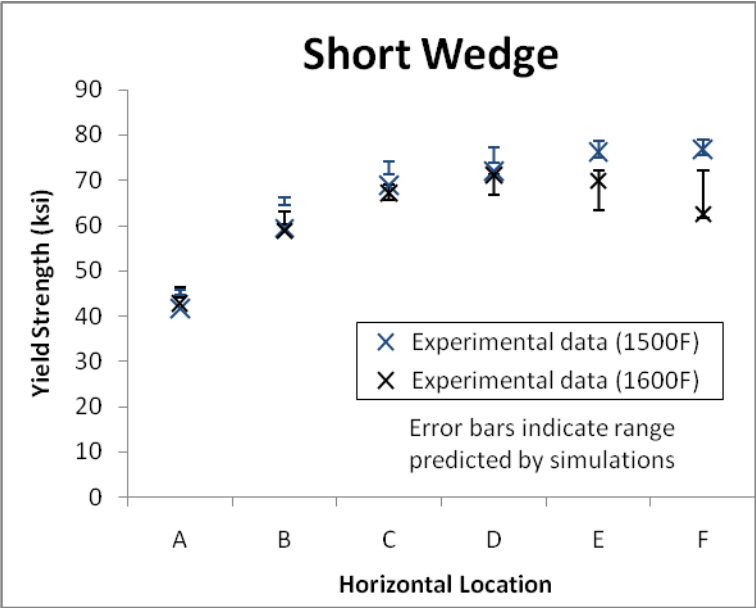

Figure 9. Final yield strengths at locations A through F of the tall wedge, based on simulation predictions and experiments.
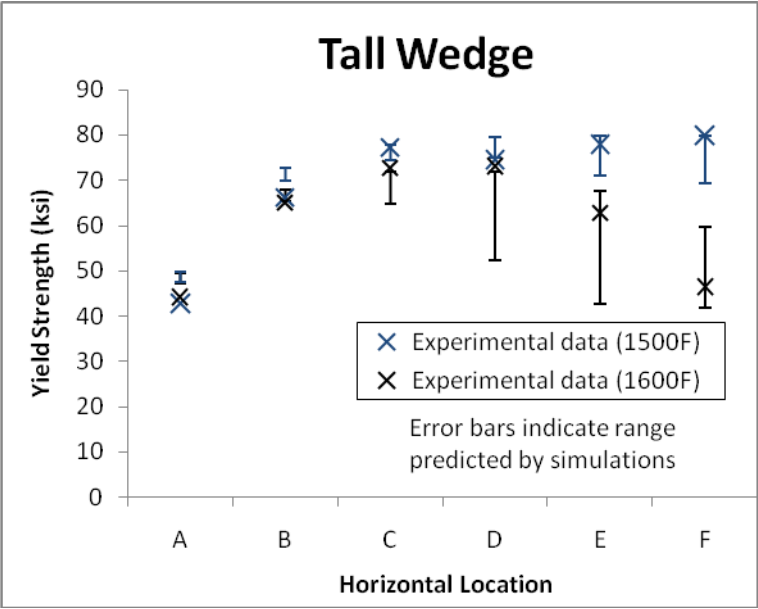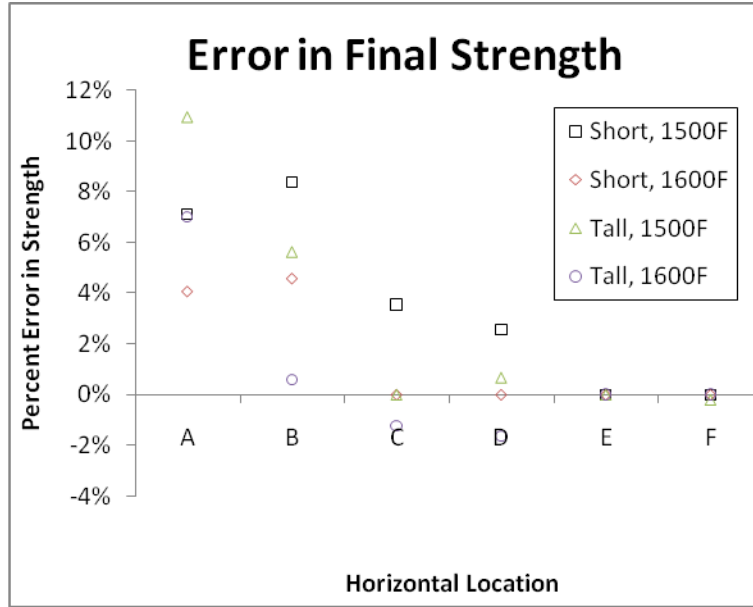
Figure 10. The error in final strength predictions.

4. Conclusions

Coupled thermal-mechanical simulations were performed to predict the final yield strength in two wedge forging geometries for two nominal temperatures. Uncertainty quantification is performed to account for unknown input parameters in the simulations. The predictions match the experimental results fairly well for all combinations of temperature and geometry.

APPENDIX

The set of parameters used in all the results presented here are as follows in SI units:

$$E = 2.00e11 - 8.70e7(\theta - 292)\,\text{Pa} \tag{8}$$

$$\mu = 8.01e10 - 3.70e7(\theta - 292)\,\text{Pa} \tag{9}$$

$$c = 0.0918 \tag{10}$$

$$n(\theta) = \frac{5700}{\theta} \tag{11}$$

$$Y(\theta) = \frac{5.27e9}{33.2 + \exp(-2.69e5/\theta)} \frac{1}{2} \tanh\left[0.00187(868 - \theta)\right]\text{Pa} \tag{12}$$

$$H(\theta) = 0.01\mu \tag{13}$$

$$R_d(\theta) = 857\exp(-5420/\theta)\,\text{Pa/K} \tag{14}$$

$$h_\zeta = 0.00167 \tag{15}$$
$$r = 1 \tag{16}$$
$$c_\theta = 5.53e4 \tag{17}$$
$$c_{\bar{\kappa}} = 0 \tag{18}$$
$$c_{\bar{\zeta}} = 9.73e17 \tag{19}$$
$$a = 0.667 \tag{20}$$
$$b = 1.33 \tag{21}$$
$$\rho = 8.00e3 \tag{22}$$
$$c_p = 667 \tag{23}$$
$$\beta = 0.95 \tag{24}$$

REFERENCES

(1) Kocks,U. F., Argon, A. S., Ashby, M. F. The Thermodynamics and Kinetics of Slip. Prog. Mater. Sci. 19, 1-291, 1975.

(2) Doherty, R.D., Hughes, D.A., Humphreys, F.J., Jonas, J.J., Jensen, D.J., Kassner, M.E., King, W.E., McNelley, T.R., McQueen, H.J., Rollett, A.D. Current issues in recrystallization: a review. Mater. Sci. Eng. A238, 219–274, 1997.

(3) Chiesa, M. L., Brown, A. A., Antoun, B. R., Ostien, J. T., Regueiro, R. A., Bammann, D. J., Yang, N. Y. Prediction of final material state in multi-stage forging processes. *AIP Conference Proceedings,* no.712, pt.1, 510-515, 2004.

(4) Haessner, F. (Ed.), Recrystallization of Metallic Materials, 2nd ed., Rieder-Verlag, Stuttgart, 1978.

(5) Humphreys, F. J., Hatherly, M. Recrystallization and Related Annealing Phenomena, Pergamon Press, Oxford, 1995.

(6) Holm, E. A., Miodownik, M. A., Rollett, A. D. On abnormal subgrain growth and the origin of recrystallization nuclei. Acta Mater. 51, 2701–2716, 2003.

(7) Doherty, R. D. Primary recrystallization. In: Cahn, R.W. et al., (Eds.), Encyclopedia of Materials: Science and Technology. Elsevier, pp. 7847–7850, 2005.

(8) Brown, A.A., Bammann, D. J., Chiesa, M. L., Winters, W.S., Ortega, A.R., Antoun, B. R., Yang, N.Y. Modeling static and dynamic recrystallization in FCC metals. In Anisotropy, Texture, Dislocations and Multiscale Modeling in Finite Plasticity & Viscoplasticity, and Metal Forming - Proceedings of PLASTICITY '06: The Twelfth International Symposium on Plasticity and its Current Applications, 2006.

(9) Brown, A.A., Bammann, D. J. A model for static and dynamic recrystallization in metals. Manuscript under revision for International Journal of Plasticity.

(10) Kocks, U. F., Mecking, H. A Mechanism for static and dynamic recovery. In: Haasen, P., Gerold, V., Kostorz, G. (Eds.), Strength of Metals and Alloys. Pergamon Press, Oxford, pp. 345–350, 1979.

(11) Kok, S., Beaudoin, A. J., Tortorelli, D. A. On the development of stage IV hardening using a model based on the mechanical threshold. Acta Mater. 50 (7), 1653-1667, 2001.

(12) SIERRA Solid Mechanics Team. Adagio 4.14 User's Guide. Sandia Report 2009-7410, 2009.

(13) Patrick K. Notz, Samuel R. Subia, Matthew M. Hopkins, Harry K. Moffat, David R. Noble. Aria 1.5 User Manual. Sandia Report 2007-2734, 2007.

(14) Qu, S., Huang, C.X., Gao, Y.L., Yang, G., Wu, S.D., Zang, Q.S., Zhang, Z.F. Tensile and compressive properties of AISI 304L stainless steel subjected to equal channel angular pressing. Matls. Sci. and Eng. A. 475, 207-216, 2008.